Original Articles

Acupuncture and Herbal Medicine

Tamarixetin suppresses neuronal ferroptosis in ischemic stroke rats by targeting and facilitating nuclear factor erythroid-2–related factor 2 expression

Yanqiu Yang[1,2], Mingxia Fang[1], Qingqi Meng[1], Yan Mi[1], Libin Xu[1], Hua Guo[1], Yueyang Liu[3], Mingzhong Li[4], Nanik Siti Aminah[5], Zipeng Gong[6,*], Yue Hou[1,*]

[1]Key Laboratory of Bioresource Research and Development of Liaoning Province, College of Life and Health Sciences, National Frontiers Science Center for Industrial Intelligence and Systems Optimization, Key Laboratory of Data Analytics and Optimization for Smart Industry, Ministry of Education, Northeastern University, Shenyang, China; [2]College of Information Science and Engineering, Northeastern University, Shenyang, China; [3]Shenyang Key Laboratory of Vascular Biology, Science and Research Center, Department of Pharmacology, Shenyang Medical College, Shenyang, China; [4]Leicester School of Pharmacy, De Montfort University, Leicester, United Kingdom; [5]Department of Chemistry, Faculty of Science and Technology, Universitas Airlangga, Surabaya, Indonesia; [6]State Key Laboratory of Discovery and Utilization of Functional Components in Traditional Chinese Medicine, Guizhou Medical University, Guiyang, China

Abstract

Objective: Neuronal ferroptosis has emerged as a promising therapeutic target for ischemic stroke. Tamarixetin, a natural dietary flavonoid, exerts protective effects against ischemic stroke by modulating neuroinflammatory responses and mitigating oxidative stress. However, its potential role in regulating neuronal ferroptosis remains unclear.

Methods: A rat model of middle cerebral artery occlusion and reperfusion and an erastin-treated SH-SY5Y cell model were used for *in vivo* and *in vitro* experiments, respectively. The neurological function of the rats was evaluated using a series of behavioral tests, the Garcia scoring system, and 2,3,5-triphenyltetrazolium chloride staining. Neuronal damage was detected *via* immunofluorescence staining and terminal deoxynucleotidyl transferase (TdT)-mediated deoxyuridine triphosphate (dUTP) nick-end labeling. Commercial kits, western blotting, and coimmunoprecipitation were used to analyze neuronal ferroptosis and the activation of the Nuclear factor erythroid-2–related factor 2 (Nrf2) signaling pathway. The direct target protein of tamarixetin was examined using the cellular thermal shift assay, drug affinity-responsive target stability assay, surface plasmon resonance, and molecular docking. Cellular Nrf2 was knocked down using small interfering RNA.

Results: Tamarixetin mitigated the neurological dysfunctions of middle cerebral artery occlusion and reperfusion (MCAO/R) rats, including motor dysfunction, limb coordination impairment, neurological deficit, cerebral infarction, and reduced neuronal loss. Furthermore, it alleviated neuronal ferroptosis *in vivo* and *in vitro* by lowering the levels of iron ions, reactive oxygen species, malondialdehyde, and acyl-CoA synthetase long-chain family member 4 and upregulating the expression of superoxide dismutase, glutathione, glutathione peroxidase 4, heme oxygenase-1, and solute carrier family 7 member 11. Tamarixetin activated the Nrf2 signaling pathway by suppressing Keap1 protein expression, weakening the interaction between Keap1 and Nrf2, upregulating Nrf2 protein expression and nuclear translocation, and promoting antioxidant response element activity. Nrf2 is the direct binding protein of tamarixetin. It specifically interacts with amino acid residues at arginine 72, arginine 515, and lysine 518. The effects of tamarixetin on Nrf2 signaling pathway activation and neuronal ferroptosis inhibition were abrogated in Nrf2 knockdown cells challenged with erastin.

Conclusions: Our findings not only identify tamarixetin as a novel ferroptosis inhibitor but also elucidate its mechanism of action *via* direct binding and Nrf2 pathway activation, providing a promising therapeutic candidate for ischemic stroke.

Keywords: Ferroptosis, Ischemic stroke, Tamarixetin, Neuron, Nuclear factor erythroid-2–related factor 2

Graphical abstract: https://links.lww.com/AHM/A203

*Corresponding authors. Yue Hou, E-mail: houyue@mail.neu.edu.cn; Zipeng Gong, E-mail: gzp4012607@126.com.

How to cite this article: *Yang YQ, Fang MX, Meng QQ, Mi Y, Xu LB, Guo H, Liu YY, Li MZ, Aminah NS, Gong ZP, Hou Y. Tamarixetin suppresses neuronal ferroptosis in ischemic stroke rats by targeting and facilitating nuclear factor erythroid-2–related factor 2 expression. Acupunct Herb Med 2026;6(1):73–90. doi: 10.1097/HM9.0000000000000182*

Received 23 July 2025 / Accepted 22 January 2026

Introduction

Ferroptosis, a recently identified form of programmed cell death, relies fundamentally on iron ions and lipid metabolism[1]. Its pathogenesis is exceedingly intricate and multifaceted, with the dysregulation of iron ions and lipid metabolism serving as crucial factors[1–2]. During ferroptosis, cellular iron levels increase and iron storage capacity decreases, ultimately resulting in excessive accumulation of iron ions[3]. Iron ions exacerbate the aberrant production of lipid reactive oxygen species (ROS), causing lipid peroxidation[4]. Concurrently, the glutathione (GSH) level is depleted, whereas the activity of GSH peroxidase 4 (GPX4) is reduced[5–6]. The presence of reduced iron promotes the conversion of ROS into hydrogen peroxide (H_2O_2) or hydroxyl radicals[7]. Excessive ROS induces oxidative stress responses that result in protein, lipid, and nucleic acid deterioration, ultimately culminating in cellular death *via* ferroptosis.

Nuclear factor erythroid 2–related factor 2 (Nrf2) is a crucial regulator of the endogenous antioxidant defense system[8]. Recently, the association between Nrf2 and ferroptosis has been extensively investigated[9]. In stressed cells, high ROS and electrophilic levels modify the cysteine residues of kelch-like ECH-associated protein 1 (Keap1), resulting in conformational changes that dissociate Keap1 from Nrf2. Changes in Keap1 slow the ubiquitination of Nrf2 and inhibit its proteasomal degradation, resulting in increased Nrf2 accumulation in the cytoplasm. The accumulated Nrf2 then enters the nucleus and initiates the transcription of downstream antioxidant genes that combat oxidative and electrophilic stress[8]. Nrf2 transcriptionally regulates nearly all genes involved in ferroptosis and plays a pivotal role in iron and lipid metabolism within cells[10]. Nrf2 activation suppresses phospholipid peroxidation and ferroptosis by boosting the expression of downstream target genes, such as *GSH* and *GPX4*[8–9,11]. Nrf2 also regulates the storage and secretion of free iron, thereby reducing intracellular iron accumulation and inhibiting ferroptosis[12]. Shin et al.[9] discovered that Nrf2 pathway inactivation increases cellular vulnerability to ferroptosis, thereby promoting its occurrence[13]. Thus, Nrf2 has emerged as a promising therapeutic target for ferroptosis inhibition.

Numerous studies have provided compelling evidence of the occurrence of ferroptosis in cerebral ischemia. Brains affected by ischemic stroke have been found to have high levels of iron ions, transferrin receptors, and iron-loaded transferrin[14–15]. Strategies for ferroptosis inhibition have yielded promising results, including reducing cerebral infarction, enhancing neurological function, and decreasing neuronal death[16–18]. These data indicate that targeting excessive ferroptosis is a promising therapeutic approach for the treatment of cerebral ischemia.

Epidemiological studies have suggested that a high dietary intake of natural flavonols is associated with a reduced incidence of cardiocerebrovascular diseases[19]. Flavonols alleviate ferroptosis through various mechanisms, including enhancing GPX4 activation, inhibiting iron uptake, and reducing ROS overproduction[20–21]. Tamarixetin, also known as 4'-O-methyl quercetin, is a naturally occurring flavonol that is widely found in fruits, vegetables, red wine, and medicinal plants[22]. Recent studies have confirmed its multifaceted pharmacological activities, including potent effects against inflammation and oxidative stress and protection against brain, heart, stomach, and liver damage[23–25]. Furthermore, tamarixetin has high *in vivo* bioavailability and the ability to cross the blood–brain barrier to access brain tissue[26]. A study showed that tamarixetin alleviated acute brain damage in animals with ischemic stroke[27]. However, the effects of tamarixetin on subacute brain injury in animals with ischemic stroke remain unclear. Studies exploring its impact on ferroptosis, a process predominantly observed during the subacute phase of ischemic stroke, are scarce. To address this, we used a rat model of middle cerebral artery occlusion and reperfusion (MCAO/R) for *in vivo* experiments and SH-SY5Y cells treated with erastin, a well-established ferroptosis inducer, for *in vitro* experiments.

Materials and methods

Reagent information

Tamarixetin (purity >98%) (JOT-12024) was obtained from Chengdu Pufeide (Chengdu, China), quercetin (purity >98%, B20527) from Shanghai Yuanye (Shanghai, China), erastin (purity >99.0%, S7242), and ferrostatin-1 (Fer-1, purity >99.0%, S7243) from Selleck (Shanghai, China); 2,3,5-triphenyltetrazolium chloride (TTC) (298-96-4), Prussian blue staining kit (G1422), and ferrous iron content commercial kit (BC5415) were acquired from SolarBio (Beijing, China). Antibodies against neuronal nuclei (NeuN, ab177487), heme oxygenase-1 (HO-1, ab13248), GPX4 (ab125066), and recombinant human Nrf2 protein (ab202153) were purchased from Abcam (Cambridge, UK). Keap1 (60027-1-Ig), Nrf2 (16396-1-AP), and β-actin (66009-1-Ig) were obtained from Proteintech (Wuhan, China), while histone H3 (#9715) was obtained from Cell Signaling Technology (Danvers, MA, USA). Commercial kits for terminal deoxynucleotidyl transferase (TdT)-mediated deoxyuridine triphosphate (dUTP) nick-end labeling (TUNEL) staining (C1089), lactate dehydrogenase (LDH) assay (C0017), and calcein AM/propidium iodide (PI) staining (C2015), nuclear- and cytoplasmic-fraction protein extraction reagents (P0028), H_2O_2 assay (S0038), superoxide dismutase (SOD, S0101) and GSH activity (S0052), malondialdehyde (MDA) content (S0131), as well as the dihydroethidium (DHE) (S0064) and 2',7'-dichlorodihydrofluorescein diacetate (DCFH-DA) probes (S0035), were purchased from Beyotime (Shanghai, China). The BODIPY 581/591 C11 staining kit (D3861) was purchased from Invitrogen (Waltham, MA, USA).

Animal surgery, groups, and treatment

Eighty-four adult Sprague-Dawley rats (male, weight 250–300 g) purchased from Liaoning Changsheng

Biotechnology (Benxi, China) were housed with free access to food and water. The suture-occluded method was employed to induce MCAO/R injury as described previously[27]. The rats in the sham group were subjected to vascular isolation without suture insertion. Seventy-two rats underwent the MCAO/R surgery. Of these, 18 rats died during or after the procedure, and six rats were excluded because of the absence of significant cerebral damage, as confirmed by postoperative neurological assessment (neurological score exceeding 10 points). The model and mortality rates were 91.7% and 25%, respectively.

The rats were divided into five groups according to the principles of blinding and randomization: sham, MCAO/R, MCAO/R + tamarixetin (10 and 20 mg/kg), and MCAO/R + quercetin (50 mg/kg). Tamarixetin and quercetin were dissolved in sodium carboxymethyl cellulose and administered to rats by gavage 3 days before and 7 days after MCAO/R surgery.

Behavioral assays

The neurobehavioral functions of the rats were evaluated in a blinded manner using the rotarod, balance beam, and corner tests, as well as neurological deficit scores after 72 hours of reperfusion.

Rotarod test

Rats were trained as described previously[28]. They underwent a 3-day training period, which consisted of three sessions per day. There was a 1-hour rest interval between sessions. The average baseline latencies of the rats during the training phase were calculated. After 24 hours of reperfusion, rats were placed on an accelerated rotarod with a 15-minute rest interval. The time at which the rats first fell was recorded. Each rat underwent three trials, and the average latency of the first fall was calculated. The latency of the rats not falling off the rotarod was recorded at 300 seconds.

Balance beam test

The rats were trained for 3 days to cross a wooden beam without falling before MCAO surgery[29]. The rats' performance in the balance beam test was evaluated 24 hours after reperfusion using a six-grade evaluation system[30]. The rats underwent the test three times, and the scores were averaged.

Corner test

The corner test was conducted as described previously[22]. The rats were placed in the device at 30°, facing the corner. All rats were retested 10 times, and turning choices were recorded. The right-turn ratio was calculated as follows: right-turn ratio = number of right turns/10 × 100.

Neurological deficit scores

The neurological function of the rats was evaluated using the Garcia scoring system[31]. The resulting scores ranged from three to 18 points. Low scores indicated poor performance.

Infarct volumes

The brain tissues were frozen at –20°C for 20 minutes and then cut into five consecutive slices. The slices were submerged in 2% TTC solution and incubated for 20 minutes at 37°C. After incubation, the brain sections were examined and the rats' infarct volumes were calculated.

Immunofluorescence staining and TUNEL staining

For assessing Nrf2 expression in neurons *in vivo*, brain sections were prepared and subjected to antigen retrieval, permeabilization, and blocking. The primary antibodies against NeuN (1:1,000) and Nrf2 (1:500) were added to the sections and incubated for 24 hours at 4°C. Sections were then washed and stained with the fluorescein isothiocyanate isomer I fluorescence antibody for 4 hours at 25°C in the dark. Subsequently, images of the brain sections were acquired and analyzed. For Nrf2 expression *in vitro*, immunofluorescence staining was performed according to a previously published protocol[32]. Neuronal death in the ischemic brain tissue was quantified using a commercial TUNEL staining kit.

Determination of iron ions

The level of iron ions was quantitatively evaluated using a Prussian blue staining kit and a commercial kit for reduced iron content. Brain sections of fresh ischemic cortical tissue were prepared and reacted with the reagents according to the manufacturer's protocol. Images of the brain sections were acquired, and the content of reduced iron per gram of protein sample was calculated.

ROS measurement

Superoxide anion levels were detected by DHE staining[33–34]. The lipid ROS levels in SH-SY5Y cells were measured *via* C11 BODIPY™ staining. SH-SY5Y cells were co-incubated with the C11 BODIPY probe (5 μM) for 30 minutes at 37°C in the dark. The cells were washed, fixed with 4% paraformaldehyde (PFA) for 30 minutes, and mounted with anti-fluorescence quenching. DHE and C11 BODIPY™ staining were examined. The H_2O_2 and ROS levels were quantified using commercially available kits. The absorbance at 560 nm (for H_2O_2) and fluorescence intensity (excitation/emission = 488/525) (for ROS) were quantified.

Oxidative and redox status determination

The MDA content and SOD and GSH activities in ischemic brain tissues and SH-SY5Y cells were accurately measured using standardized protocols for each commercial kit.

Cell treatment and cellular viability

SH-SY5Y cells were cultured in Dulbecco's modified Eagle's medium containing 10% fetal bovine serum and 1% penicillin–streptomycin. The cells were pretreated with tamarixetin (1, 10, and 30 μM), quercetin (80 μM), or Fer-1 (5 μM) for 2 hours and then exposed to erastin (5 μM) for 24 hours.

The viability of SH-SY5Y cells was evaluated using the 3-(4,5-dimethylthiazol-2-yl)-2,5 diphenyltetrazolium bromide (MTT) assay[35], a commercial LDH kit, and calcein AM/PI staining[36]. For the MTT assay, cells were exposed to MTT (0.25 mg/mL) and incubated for 4 hours at 37°C under light-restricted conditions. The cells were then dissolved in dimethyl sulfoxide (DMSO), and the absorbance at 490 nm was quantified. For the LDH assay, the cells were centrifuged at 400 g for 5 minutes, followed by a 1-hour co-incubation with LDH reagents (37°C) and then centrifugation (400 g for 5 minutes). For calcein AM/PI staining, the cells were stained with calcein AM (1 μM) and PI probe (1 μM) at 37°C for 1 hour. Images of the cells were acquired.

Western blotting

The lysed proteins from ischemic brain tissues and SH-SY5Y cells were isolated, and the nuclear and cytoplasmic fractions were extracted and quantitatively analyzed using the bicinchoninic acid method. Protein samples were resolved by sodium dodecyl sulfate–polyacrylamide gel electrophoresis and transferred onto polyvinylidene fluoride membranes. Subsequently, the membranes were incubated with primary antibodies against Nrf2 (1:1,000), Keap1 (1:1,000), HO-1 (1:1,000), GPx4 (1:1,000), β-actin (1:10,000), and histone H3 (1:1,000) for 24 hours at 37°C. Membranes were probed with horseradish peroxidase-conjugated secondary antibodies. The target proteins were visualized, and their relative expression was quantified *via* normalization to β-actin or histone H3.

Coimmunoprecipitation analysis

Coimmunoprecipitation experiments were conducted as previously described[37]. Briefly, protein samples were extracted from SH-SY5Y cells and divided into two portions. One portion served as the input control, whereas the other was subjected to overnight incubation with the Keap1 primary antibody at 4 °C, followed by incubation with protein A/G agarose beads (Beyotime, P2055) or IgG overnight at 4°C. Subsequently, the protein complexes were washed and analyzed by western blotting.

Small-interfering RNA transfection

Commercial small-interfering RNA (siRNA) targeting Nrf2 was synthesized by GenePharma (Wuhan, China). The primer sequences were 5'-GAAUGGUCCUAAAACACCA-3' (Nrf2 siRNA sense), 5'-UGGUGUUUUAGGACCAUUC-3' (Nrf2 siRNA antisense), 5'-GAAUGGUCCUAAAACACCA-3' (negative siRNA sense), and 5'-UGGUGUUUUAGGACCAUUC-3' (negative siRNA antisense). SH-SY5Y cells were incubated with Nrf2 siRNA for 60 hours and treated with erastin for 24 hours, with or without a 2-hour tamarixetin pretreatment.

Cellular thermal shift assay

The cellular thermal shift assay was performed as previously described[38]. Briefly, the SH-SY5Y cells were incubated with tamarixetin or DMSO for 2 hours, collected, lysed in liquid nitrogen, and centrifuged. The supernatants were equally divided, heated at different temperatures (46°C–66°C), and then centrifuged. The supernatants were collected and analyzed.

Drug affinity responsive target stability assay

The drug affinity responsive target stability assay was performed as previously described[39]. Briefly, SH-SY5Y cells were lysed using protease lysis buffer. The lysates were aliquoted and incubated with tamarixetin or DMSO for 1 hour. The samples were then proteolyzed and centrifuged, and the supernatants were analyzed.

Molecular docking

The interaction between tamarixetin and Nrf2 was analyzed using molecular docking[40]. Briefly, the structure of Nrf2 (PDB ID: 7X5G) was obtained from the RCSB Protein Data Bank (http://www.rcsb.org/). The protein structure was prepared using PyMOL 2.5.2, with water molecules and heteroatoms removed, and stored in a.pdb format. The 3D chemical structure of tamarixetin (CID: 5281699) was downloaded from PubChem (https://pubchem.ncbi.nlm.nih.gov/). AutoDock Vina and PyMOL 2.5.2 were used to perform molecular docking. The grid box was centered on the active site of the protein, with dimensions set to 30 Å × 30 Å × 30 Å. Visualization of the docking poses and interaction analysis were performed using Discovery Studio software.

Surface plasmon resonance

The interaction between tamarixetin and Nrf2 was evaluated using a Biacore T200 system following the manufacturer's instructions[41].

Statistical analysis

Data were expressed as the mean ± standard error of the mean and analyzed using SPSS version 25.0. One-way analysis of variance, followed by Tukey's *post hoc* test, was used for comparisons among multiple groups under a single experimental condition. An unpaired Student's *t* test was used for comparisons between two groups. For experiments involving two independent variables, two-way analysis of variance was employed. Statistical significance was set at $P < 0.05$.

Results

Tamarixetin alleviated the brain injuries in MCAO/R rats

An MCAO/R rat model was developed to evaluate the efficacy of tamarixetin in treating brain injury resulting from ischemic and reperfusion (I/R). The rats were administered tamarixetin and quercetin, as illustrated in Figure 1B. Neurological functions of the rats were comprehensively evaluated using a battery of behavioral tests consisting of motor function and limb coordination evaluations. The collected data indicated that, compared with the rats in the sham group, MCAO/R rats demonstrated poorer performance, characterized by reduced latency times in the rotarod test (Figure 1C), higher balance scores in the beam balance test (Figure 1D), a higher right-turning tendency in the corner test (Figure 1E), and lower neurological deficit scores (Figure 1F). In addition, MCAO/R rats had larger cerebral infarct volumes (Figure 1G and H). As illustrated in Figure 1C–F, tamarixetin (10 and 20 mg/kg) and quercetin markedly increased the behavioral test scores in MCAO/R rats. Furthermore, cerebral infarction analysis revealed that cerebral infarct volume was reduced after treatment with tamarixetin (10 and 20 mg/kg) and quercetin (Figure 1G and H). These findings indicated that tamarixetin exerts a beneficial effect on neurological dysfunction in MCAO/R rats, particularly with regard to motor disability, limb incoordination, neurological problems, and brain infarction.

Subsequently, neuronal expression in the cortex and striatum, areas that govern motor function and limb coordination, was analyzed. Notably, the poor performance of MCAO/R rats in behavioral tests was associated with a decrease in NeuN-positive cells and an increase in TUNEL-positive cells (Figure 1I and J). Interestingly, in MCAO/R rats treated with tamarixetin and quercetin, a notable increase in the number of mature neurons was observed, as evidenced by a greater abundance of NeuN-stained cells and concurrent reduction in apoptotic neurons, as indicated by a low number of TUNEL-positive cells (Figure 1I and J). These findings suggest that tamarixetin and quercetin effectively reduced neuronal loss in MCAO/R rats. Collectively, our data highlight the neuroprotective effects of tamarixetin on the alleviation of brain injury resulting from I/R in ischemic stroke.

Tamarixetin reduced ferroptosis in the MCAO/R rats

To comprehensively evaluate the fundamental mechanisms underlying the therapeutic effects of tamarixetin in the MCAO/R rats, we explored the impact of tamarixetin on ferroptosis. Initially, the expression of iron ions, ROS, acyl-CoA synthetase long-chain family member 4 (ASCL4), and solute carrier family 7 member 11 (SLC7A11), which are key hallmarks of ferroptosis, was evaluated. Our results indicated a higher prevalence of iron deposits in the ischemic cortex and striatum of MCAO/R rats than in the sham group (Figure 2A). Interestingly, this effect was attenuated by treatment with tamarixetin (10 and 20 mg/kg) and quercetin (Figure 2A). Furthermore, tamarixetin (10 and 20 mg/kg) and quercetin reduced the iron ion levels in the brains of MCAO/R rats (Figure 2B). In addition, we analyzed the association between reduced iron ion levels and neurological impairment. We observed a negative correlation between the reduced iron ion content and latency time in the rotarod test, neurological deficit scores, and NeuN fluorescence intensity in the ischemic cortex (Figure 2C). Conversely, we found a positive correlation among the scores in the beam balance test, the right-turning tendency in the corner test, and TUNEL-positive cell counts (Figure 2C). These findings suggest that a reduction in iron ion accumulation markedly contributes to the amelioration of neurological impairments in MCAO/R rats.

Furthermore, we quantified the ROS levels *in vivo*. As illustrated in Figure 2D–F, MCAO/R rats exhibited increased DHE fluorescence in the ischemic cortex and striatum, higher H_2O_2 content, and greater DCFH-DA RFU than those of rats in the sham group. However, these increases were significantly reduced by tamarixetin (10 and 20 mg/kg) and quercetin treatments. Regarding lipid peroxidation, tamarixetin (10 and 20 mg/kg) and quercetin effectively decreased MDA content in the ischemic cortex of MCAO/R rats (Figure 2G). Our findings suggest that tamarixetin (10 and 20 mg/kg) and quercetin reversed the downregulation of SOD activity and GSH content caused by MCAO/R (Figure 2H and I). Specifically, they upregulated the expression of HO-1 and GPx4 in MCAO/R rats (Figure 2J and K). Moreover, tamarixetin treatment reduced the protein level of ASCL4 while upregulating SLC7A11 expression [Supplementary Figure S1A and B, https://links.lww.com/AHM/A202]. Collectively, these results indicate the inhibitory effects of tamarixetin on ferroptosis in MCAO/R rats, suggesting its potential as a primary preventive agent against neurological dysfunction associated with ischemic stroke.

Tamarixetin suppressed neuronal ferroptosis in vitro

To examine the effects of tamarixetin on neuronal ferroptosis, SH-SY5Y cells were incubated with erastin, an inducer of ferroptosis *in vitro*. Compared with control cells, cells treated with erastin exhibited a decreased survival rate, as evidenced by diminished cellular viability (Figure 3A), elevated LDH levels (Figure 3B), reduced calcein AM RFU, and increased PI RFU (Figure 3C and D). Notably, tamarixetin (10 and 30 μM) mitigated these changes (Figure 3A–D), resembling the effects of quercetin and Fer-1. Moreover, the level of reduced C11 BODIPY™ was lower, whereas the oxidized form was higher in erastin-incubated cells than in the control cells. This was further corroborated by the increase in H_2O_2 content and DCFH-DA RFU, as shown in Figure 4A–C, both of which indicated excessive generation of lipid ROS. Consistent with this observation, the MDA content also increased after incubation with erastin (Figure 4D). These findings strongly indicated lipid peroxidation, which was successfully suppressed by tamarixetin (10 and 30 μM), quercetin, and Fer-1 treatments (Figure 4A–D). Figure 4E shows the expression of the reduced iron ions. Notably, the levels of reduced iron ions were found to be lower in tamarixetin-treated (1,

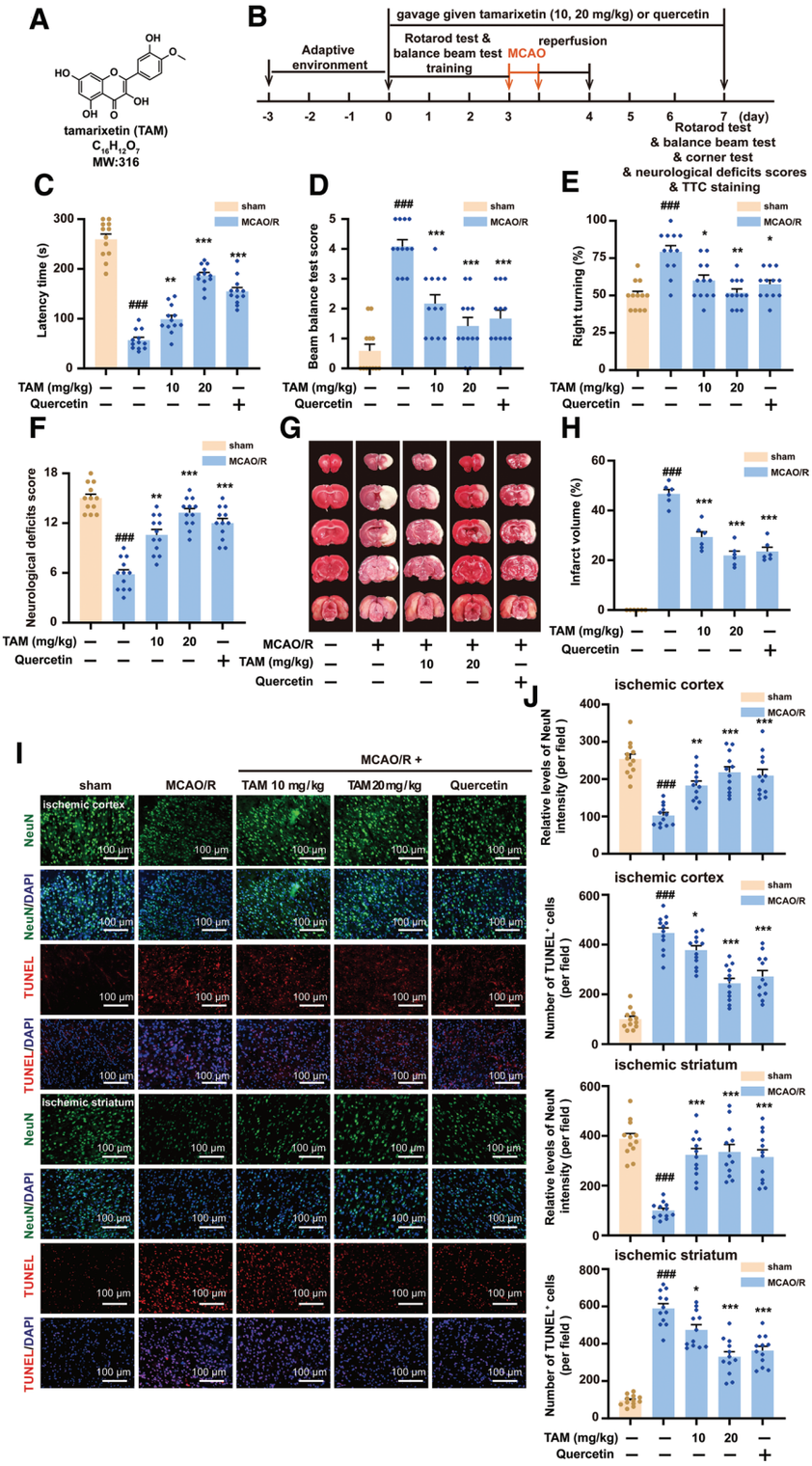

Figure 1. Tamarixetin alleviated neurological dysfunction and reduced neuronal loss in MCAO/R rat models. (A) Chemical structure of tamarixetin. (B) Experimental design for the animal studies. The rats' neurological functions were rigorously evaluated through a series of behavioral tests. This included measurement of the latency time in the rotarod test (C), scoring performance in the balance beam test (D), evaluation of right-turning performance in the corner test (E), and determination of neurological deficits using the Garcia scoring system (F). Each group comprised 12 rats. Brain infarctions were identified *via* TTC staining; representative images and quantitative data are presented (G–H). $N = 6$ rats in each group. The neuronal expression in the ischemic cortex and striatum was evaluated *via* NeuN and TUNEL staining. Typical images of NeuN and TUNEL staining, along with the corresponding statistical analysis, are presented (I–J). $N = 12$ from 3 rats in each group; scale bar = 100 μm. Values are expressed as mean ± SEM. $^{###}P < 0.001$ *vs*. sham group; $^{*}P < 0.05$, $^{**}P < 0.01$, and $^{***}P < 0.001$ *vs*. MCAO/R group. dUTP: Deoxyuridine triphosphate; MCAO/R: Middle cerebral artery occlusion and reperfusion; SEM: Standard error of mean; TdT: Terminal deoxynucleotidyl transferase; TTC: 2,3,5-triphenyltetrazolium chloride; TUNEL: TdT-mediated dUTP nick-end labeling.

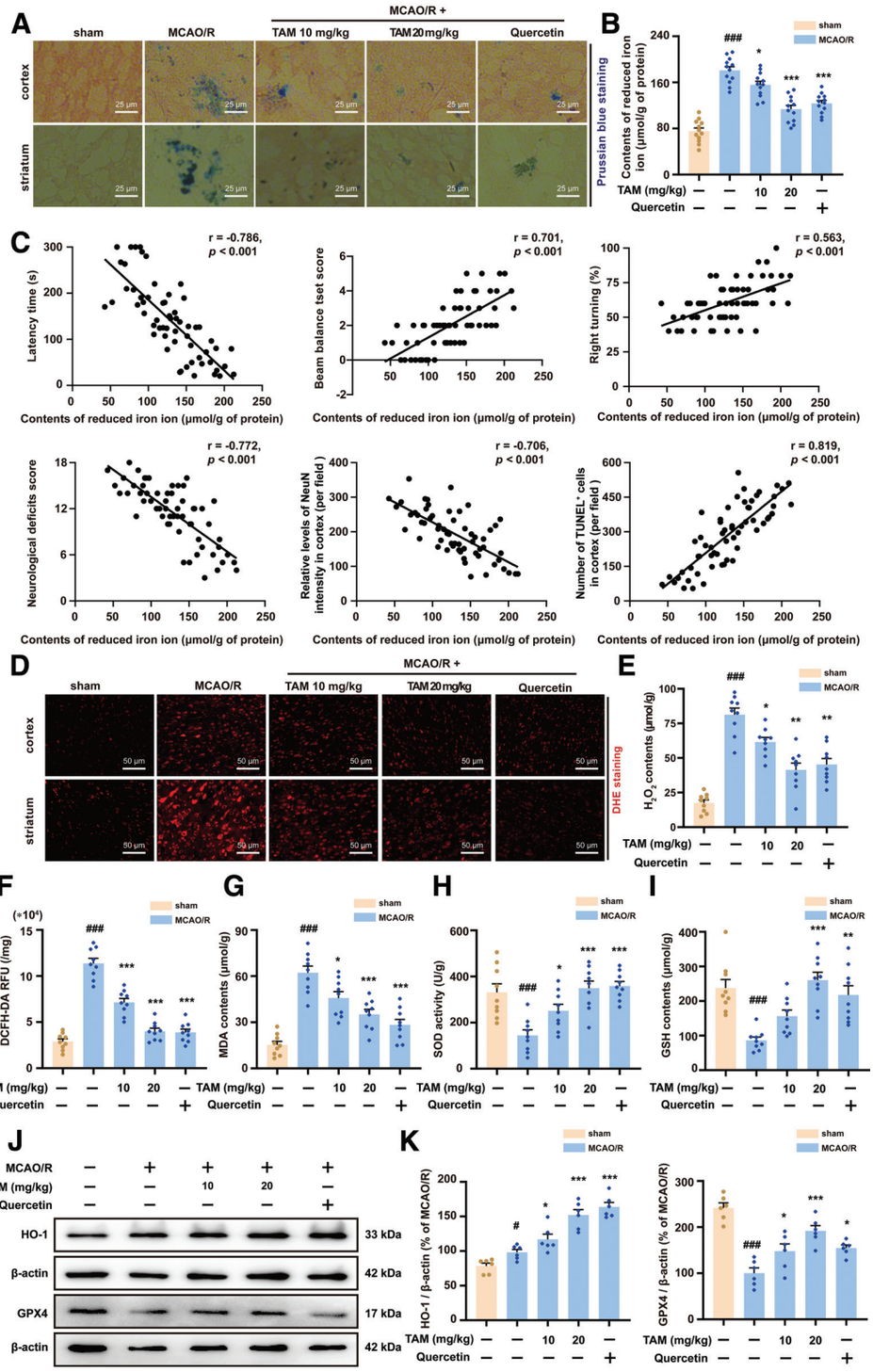

Figure 2. Tamarixetin suppressed ferroptosis in MCAO/R rats. Accumulations of iron ions in the ischemic cortex and striatum were visualized *via* Prussian blue staining, with representative images presented (A) (*N* = 3 rats per group). (B) The reduced iron ion contents in the ischemic cortex were quantitatively measured using a commercial kit (*N* = 12 from 3 rats in each group). Pearson's correlation analysis was conducted to evaluate the association between reduced iron ion content and various neurological and biochemical parameters, including latency time in the rotarod test, scores from the balance beam test, right-turning tendency in the corner test, neurological deficit scores, NeuN fluorescence intensity, and TUNEL$^+$ cell counts (C). Superoxide anion was labeled using the DHE probe. Representative images and quantitative analysis of DHE staining are presented (D). *N* = 9 from 3 rats per group; scale bar = 100 μm. The H_2O_2 content was detected using a commercial kit (E) (*N* = 9 obtained from 3 rats in each group). Intracellular ROS were stained with the DCFH-DA probe (F) (*N* = 9 from 3 rats per group). The MDA content (G), SOD activity (H), and GSH content (I) were quantified using commercial kits (*n* = 9 samples collected from 3 rats in each group). The protein expression of HO-1 and GPx4 was detected *via* western blotting, and representative immunoblot band images along with statistical analysis are presented (J–K) (*N* = 6 from 3 rats per group). Values are expressed as mean ± SEM. $^{\#}P < 0.05$ and $^{\#\#\#}P < 0.001$ *vs*. sham group; $^{*}P < 0.05$, $^{**}P < 0.01$, and $^{***}P < 0.001$ *vs*. MCAO/R group. DCFH-DA: 2',7'-Dichlorodihydrofluorescein diacetate; DHE: Dihydroethidium; dUTP: Deoxyuridine triphosphate; GPX4: Glutathione peroxidase 4; GSH: Glutathione; HO-1: Heme oxygenase-1; MCAO/R: Middle cerebral artery occlusion and reperfusion; MDA: Malondialdehyde; ROS: Reactive oxygen species; SEM: Standard error of mean; SOD: Superoxide dismutase; TdT: Terminal deoxynucleotidyl transferase; TUNEL: TdT-mediated dUTP nick-end labeling.

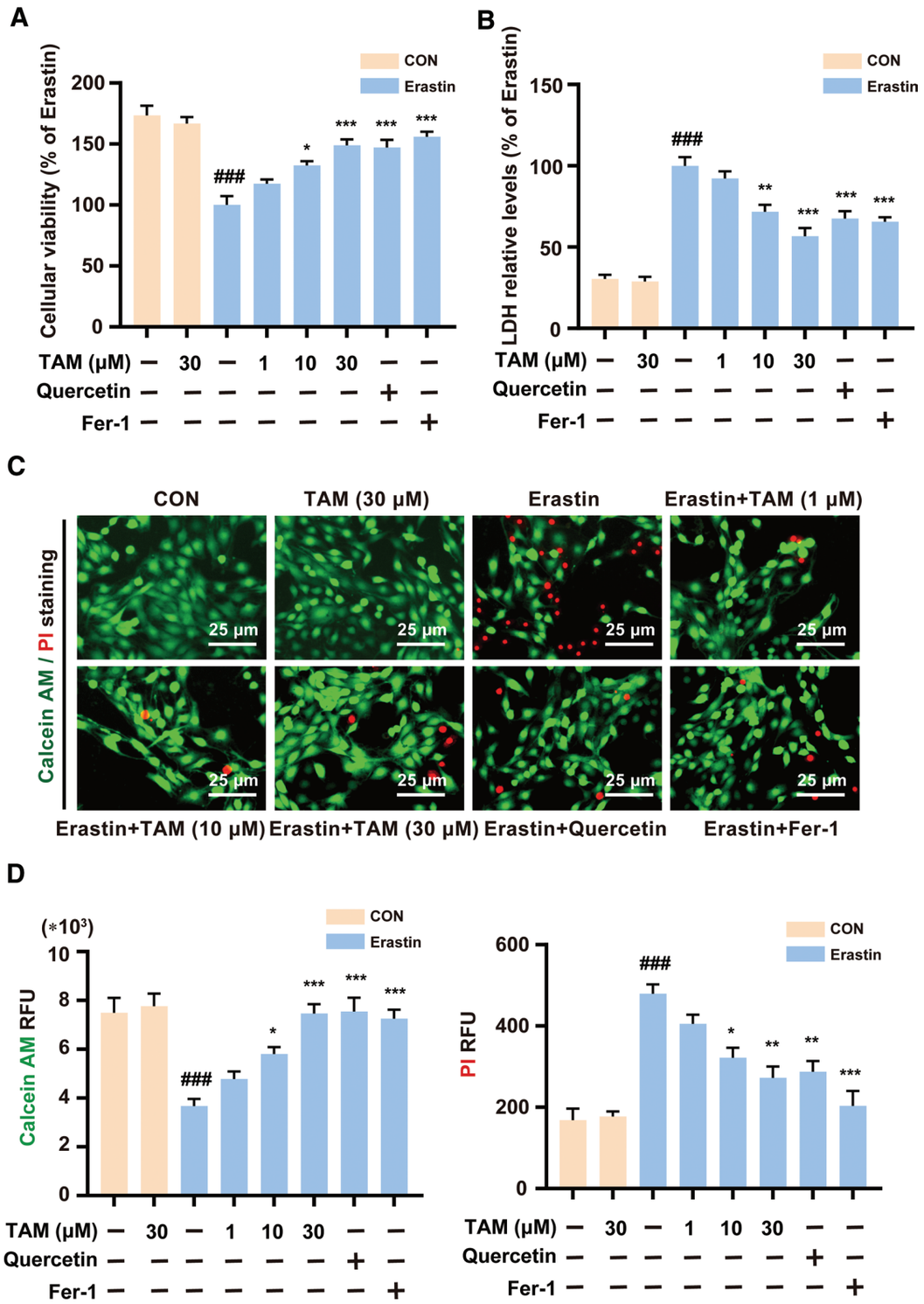

Figure 3. Tamarixetin reduced erastin-induced cellular death in SH-SY5Y cells. Cellular viability was detected using MTT assay, LDH commercial kit, and calcein AM/PI staining. The cellular viability (A), LDH levels in supernatants (B), and typical images of calcein AM and PI staining, accompanied by quantitative analysis (C–D), are presented. $N = 3$ in each group; scale bar = 100 μm. Data are expressed as mean ± SEM. $^{\#}P < 0.05$, $^{\#\#}P < 0.01$, $^{\#\#\#}P < 0.001$ *vs*. control group; $^{*}P < 0.05$, $^{**}P < 0.01$, and $^{***}P < 0.001$ *vs*. erastin group. LDH: Lactate dehydrogenase; MTT: 3-(4,5-dimethylthiazol-2-yl)-2,5 Diphenyltetrazolium bromide; PI: Propidium iodide; SEM: Standard error of mean; TAM: Tamarixetin.

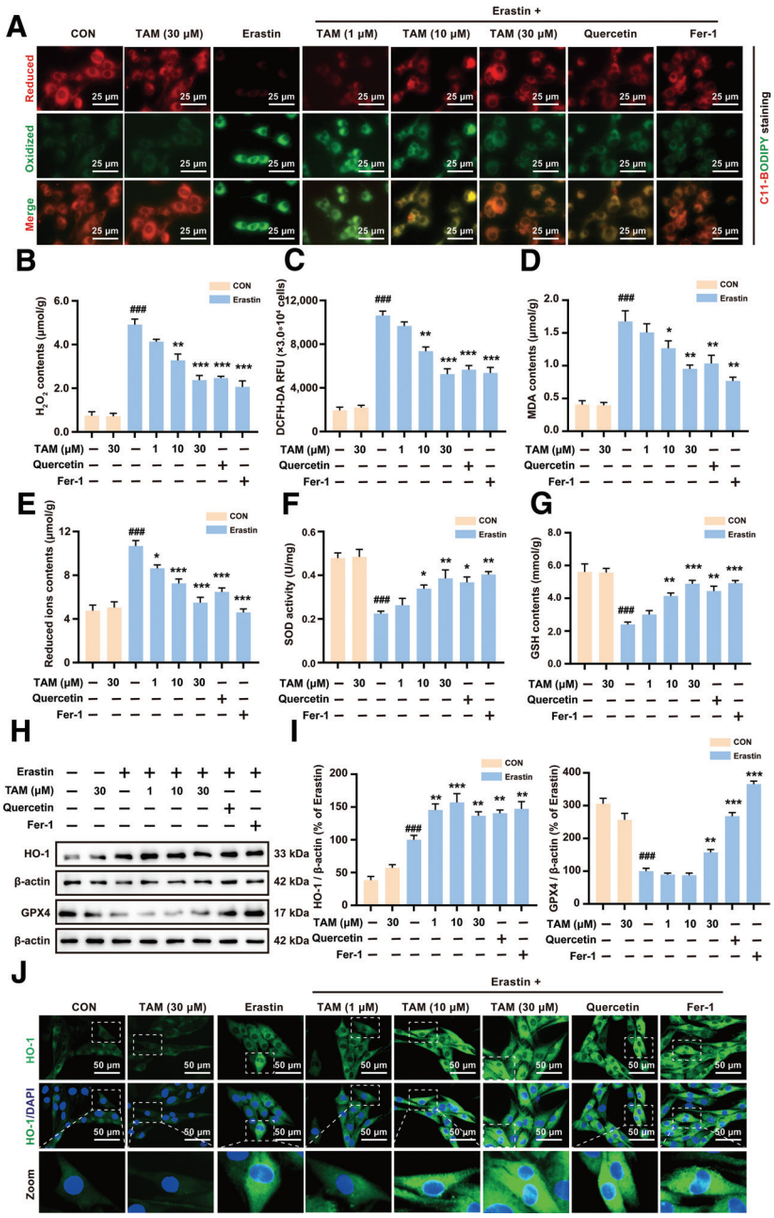

Figure 4. Tamarixetin inhibited erastin-induced neuronal ferroptosis *in vitro*. To evaluate lipid ROS generation, C11-BODIPY™ staining was employed, and representative images along with quantitative analyses of the staining are displayed (A). $N = 3$ in each group; scale bar = 50 μm. Commercial kits were used to evaluate various parameters, including H_2O_2 content (B), DCFH-DA relative fluorescence unit (C), MDA content (D), reduced iron ion level (E), SOD activity (F), and GSH content (G). $N = 3$ per group. Western blotting was conducted to evaluate the protein expression of GPx4, whereas the level of HO-1 protein was examined *via* western blotting and immunofluorescence staining. The images of GPx4 and HO-1 immunoblot bands, statistical analysis of protein expression (H–I), and HO-1 staining images are presented for analysis (J). $N = 3$ from each group; scale bar = 50 μm. Data are expressed as mean ± SEM. $^{\#}P < 0.05$, $^{\#\#}P < 0.01$, $^{\#\#\#}P < 0.001$ *vs*. control group; $^{*}P < 0.05$, $^{**}P < 0.01$, and $^{***}P < 0.001$ *vs*. erastin group. DCFH-DA: 2',7'-Dichlorodihydrofluorescein diacetate; GPX4: Glutathione peroxidase 4; GSH: Glutathione; HO-1: Heme oxygenase-1; MDA: Malondialdehyde; ROS: Reactive oxygen species; SEM: Standard error of mean; SOD: Superoxide dismutase; TAM: Tamarixetin.

10, and 30 μM) cells than in erastin-treated cells. Similar inhibitory effects on the abnormal expression of reduced iron ions were observed following treatment with quercetin and Fer-1 (Figure 4E). To further investigate the effects of tamarixetin on neuronal ferroptosis, we evaluated cellular antioxidant capacity. Our findings indicated significant downregulation of SOD activity, GSH content, and GPx4 protein expression in erastin-treated cells compared with observations in control cells, coupled with the upregulation of HO-1 protein expression (Figure 4F–J). However, treatment with tamarixetin, quercetin, and Fer-1 reversed the downregulation of SOD activity, GSH content, and GPx4 protein expression (Figure 4F–I). Tamarixetin treatment further augmented HO-1 expression (Figure 4H and J). In addition, tamarixetin treatment downregulated ASCL4 protein levels in erastin-treated cells and upregulated SLC7A11 protein levels [Supplementary Figure S1C and D, https://links.lww.com/AHM/A202]. Collectively, our data indicate that tamarixetin exerts an inhibitory effect on neuronal ferroptosis *in vitro*.

Tamarixetin activated the Nrf2 pathway in vivo and in vitro

In the following section, we examine the expression of Nrf2, a crucial modulator of ferroptosis. Our findings indicated that, in comparison with sham group rats, MCAO/R rats displayed a low level of Keap1 protein expression and a high level of Nrf2 protein expression (Figure 5A and B). The upregulation of Nrf2 expression was further corroborated by immunofluorescence staining, which revealed high-intensity green fluorescence in the neuronal compartments (Figure 5C). Regarding spatial distribution, we observed an increased translocation of Nrf2 into the neuronal nucleus, as evidenced by the prominent colocalization of Nrf2 (green), NeuN (red), and 4',6-diamidino-2-phenylindole (DAPI) (blue) staining patterns (Figure 5C). Following treatment with tamarixetin (10 and 20 mg/kg) and quercetin, we observed a further reduction in Keap1 protein levels, accompanied by the upregulation of Nrf2 protein levels and its nuclear translocation (Figure 5A–C). *In vitro*, compared with control cells, erastin-induced cells exhibited downregulated Keap1 protein levels, along with upregulated Nrf2 protein expression. These alterations were further enhanced by treatment with tamarixetin, quercetin, or Fer-1 (Figure 5D and E). Coimmunoprecipitation assay data revealed that tamarixetin further attenuated the binding affinity between Nrf2 and Keap1 in erastin-treated cells (Figure 5F and G). *In vitro* experiments revealed that cells treated with erastin displayed a reduction in Nrf2 expression in the cytoplasm and an elevation in the nucleus (Figure 5H and I). Moreover, tamarixetin treatment suppressed Nrf2 expression in the cytoplasm and enhanced its nuclear expression (Figure 5H and I). Immunofluorescence analysis corroborated these findings, demonstrating that tamarixetin promoted the colocalization of Nrf2 with DAPI in erastin-treated cells (Figure 5J). Collectively, these results indicate that tamarixetin activates the Keap1–Nrf2 pathway, suppressing ferroptosis *in vivo* and *in vitro*.

Nrf2 was the direct protein target of tamarixetin

To elucidate the precise mechanism by which tamarixetin regulates the Keap1–Nrf2 pathway and suppresses ferroptosis, we identified the cellular protein targets of tamarixetin. As illustrated in Figure 6A, compared with observations in the control group, the protein level of Nrf2 was significantly reduced in the presence of pronase. Tamarixetin treatment reversed this downregulation and, interestingly, a high dose was correlated with a more favorable outcome. Tamarixetin has been suggested to enhance the enzymatic stability of Nrf2. Compared with observations in the control group, the protein level of Nrf2 incubated with tamarixetin increased after exposure to a temperature gradient ranging from 46°C to 61°C (Figure 6B). This suggests that tamarixetin treatment enhanced the thermal stability of Nrf2. To further validate the direct interaction between tamarixetin and Nrf2, a surface plasmon resonance assay was performed to analyze binding affinity. The results indicated that tamarixetin interacted with Nrf2 protein, with an equilibrium constant (K_D) of 105.30 μM (Figure 6C and D). Molecular docking was performed to elucidate the interactions between tamarixetin and Nrf2. Our findings indicated that tamarixetin interacted with Nrf2 (PDB ID: 7X5G), specifically at the amino acid residues arginine 72, arginine 515, and lysine 518 (Figure 6E), and the binding energy was −7.290 kcal/mol (Figure 6E). Collectively, our findings indicate that Nrf2 is a direct target of tamarixetin.

Nrf2 silence weakened the effects of tamarixetin on ferroptosis

To establish the inhibitory effect of tamarixetin against the ferroptosis mediated by Nrf2, we silenced Nrf2 expression in SH-SY5Y cells using an siRNA reagent, and the knockdown efficiency was subsequently validated *via* western blot analysis, as illustrated in Figure 7A and B. Accordingly, we analyzed the spatial distribution of Nrf2 *via* western blotting and immunofluorescence staining. Our observations indicated downregulation of Nrf2 expression in the nucleus after Nrf2 silencing (Figure 7C–E). In addition, the stimulatory effects of tamarixetin on Nrf2 protein expression and nuclear translocation were alleviated in erastin-treated SH-SY5Y cells (Figure 7C–E). Subsequently, we evaluated the viability of SH-SY5Y cells with silenced Nrf2 expression and observed a considerable decrease in the relative cellular survival rate. As illustrated in Figure 8A–D, such a decline was evident from the reduced cellular viability in the MTT assay, high LDH levels in the LDH release assay, and diminished calcein fluorescence intensity in calcein staining. Under these conditions, the stimulatory effects of tamarixetin on cell viability were markedly reduced or completely eliminated (Figure 8A–D).

Compared with the negative siRNA treatment, Nrf2 siRNA treatment decreased the level of reduced C11 BODIPY™ (red signal) and increased the level of oxidized C11 BODIPY™ (green signal) in cells incubated with erastin (Figure 8E). We also observed increased ROS and MDA levels (Figure 8F and G). The inhibitory effects of tamarixetin on reduced C11 BODIPY™ levels, ROS levels, and MDA content were diminished

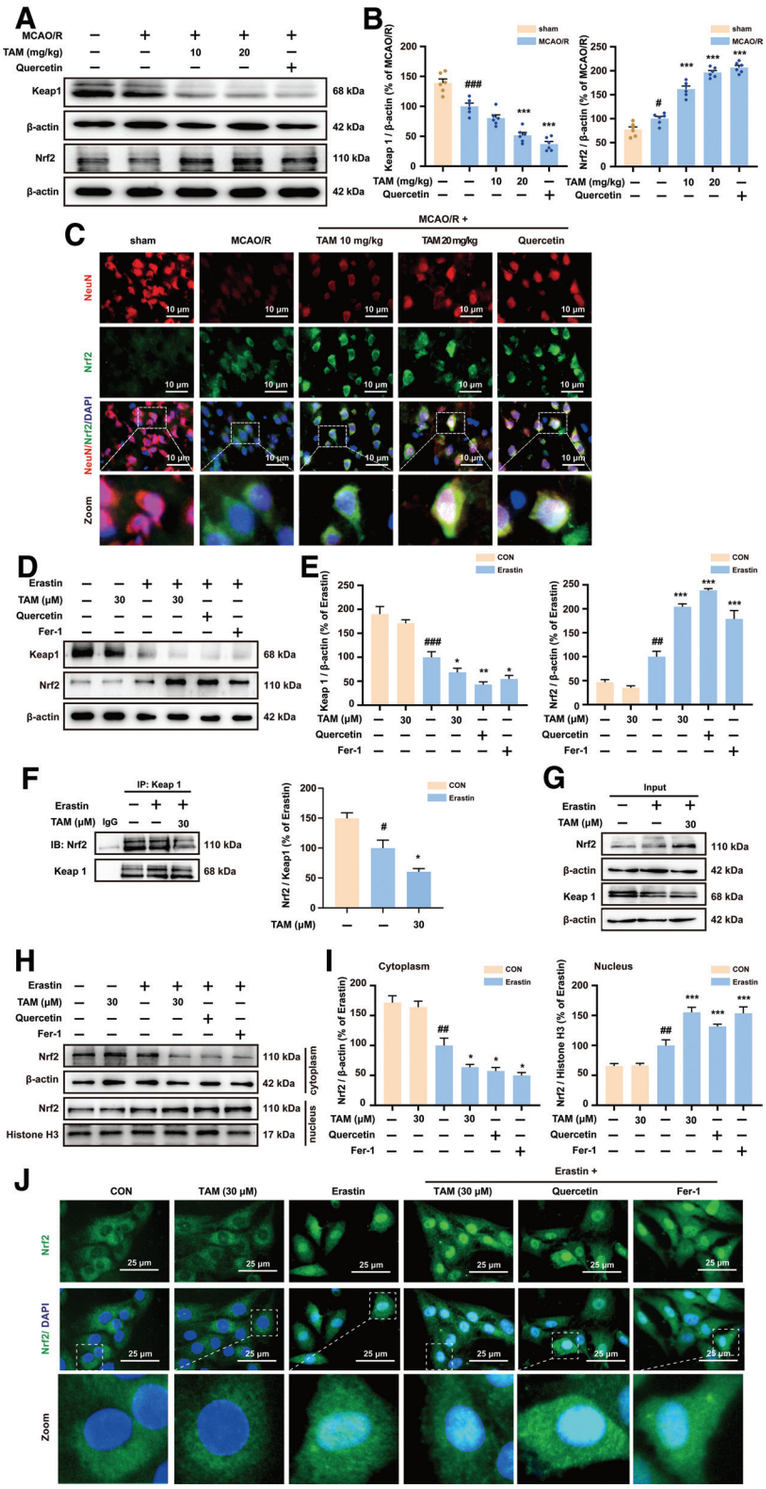

Figure 5. Tamarixetin activated the Nrf2 pathway *in vivo* and *in vitro*. Western blotting was employed to evaluate the protein expression of Keap1 and Nrf2. Representative images of the Keap1 and Nrf2 immunoblot bands, along with their corresponding statistical analyses, are presented (A–B for *in vivo*, D–E for *in vitro*). $N = 6$ from 3 rats *in vivo* and $N = 3$ *in vivo*. The expression of Nrf2 in neurons *in vivo* was evaluated *via* NeuN and Nrf2 double immunofluorescence staining, and representative images are presented (C). $N = 3$ rats; scale bar = 10 μm. The nucleus translocation of Nrf2 in SH-SY5Y cells was evaluated *via* western blotting and immunofluorescence staining. Representative images, along with their statistical analyses, are provided for analysis (H–J). $N = 3$ in each group. The interaction between Nrf2 and Keap1 was measured *via* Co-IP assay. Typical immunoblot images, along with statistical analysis, are presented (F–G). $N = 3$ in each group. Data are expressed as mean ± SEM. $^{\#}P < 0.05$, $^{\#\#}P < 0.01$, $^{\#\#\#}P < 0.001$ *vs*. sham or control group; $^{*}P < 0.05$, $^{**}P < 0.01$ and $^{***}P < 0.001$ *vs*. MCAO/R or erastin group. Keap1: Kelch-like ECH-associated protein 1; MCAO/R: Middle cerebral artery occlusion and reperfusion; SEM: Standard error of mean; TAM: Tamarixetin.

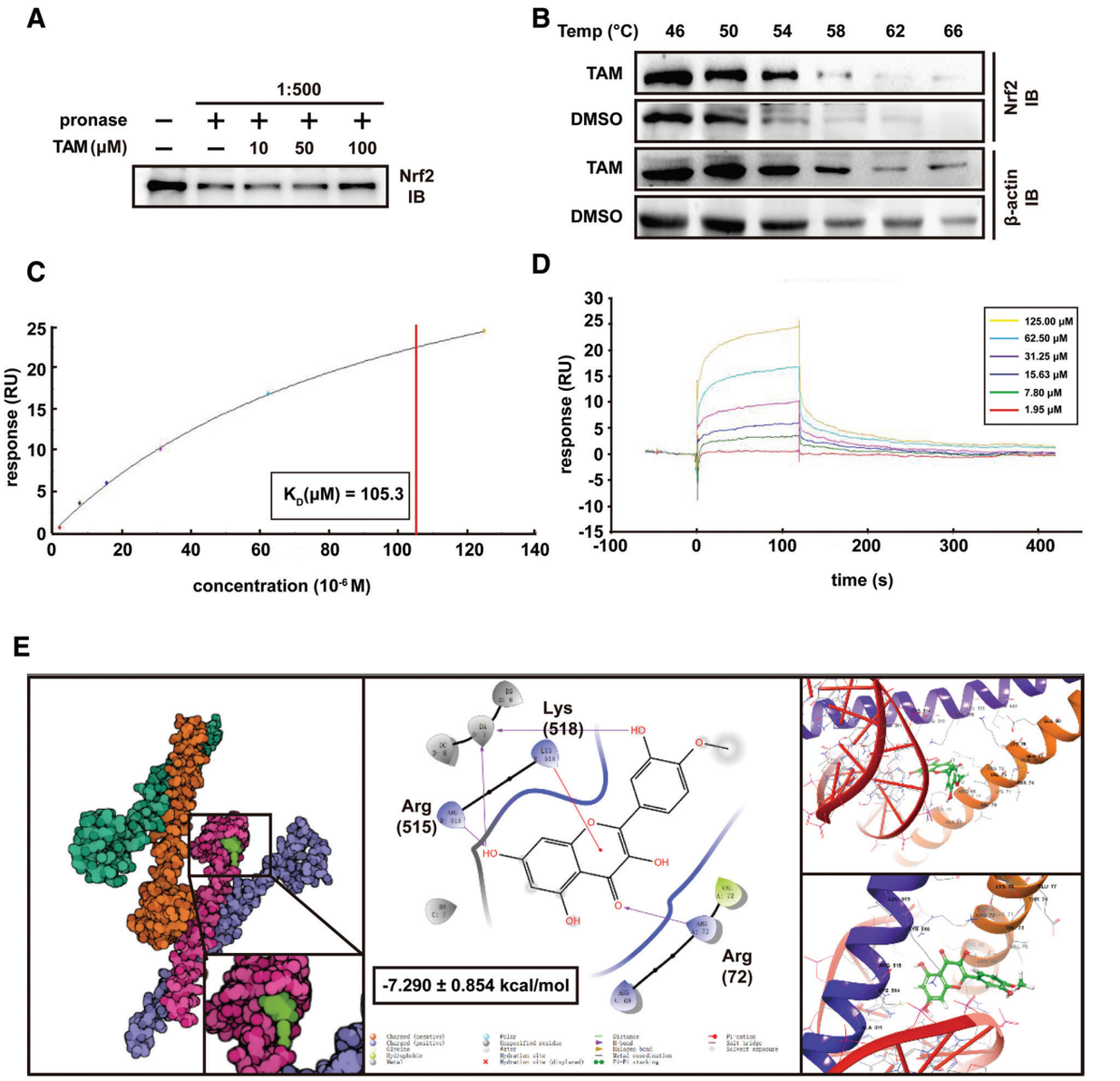

Figure 6. Nrf2 is the direct target protein of tamarixetin. The enzymatic stability of tamarixin was evaluated *via* DARTS assay. Representative immunoblot images are presented (A). The thermal stability of tamarixin under temperature gradient from 46°C to 66°C was tested *via* CETSA assay. Typical immunoblot band images and quantitation are illustrated (B). The direct binding between tamarixetin and Nrf2 was analyzed *via* SPR. The affinity (K_D) is shown (C–D). Details of the interaction were analyzed *via* molecular docking (E). CETSA: Cellular thermal shift assay; DARTS: Drug affinity responsive target; DMSO: dimethyl sulfoxide; SPR: Surface plasmon resonance; TAM: Tamarixetin.

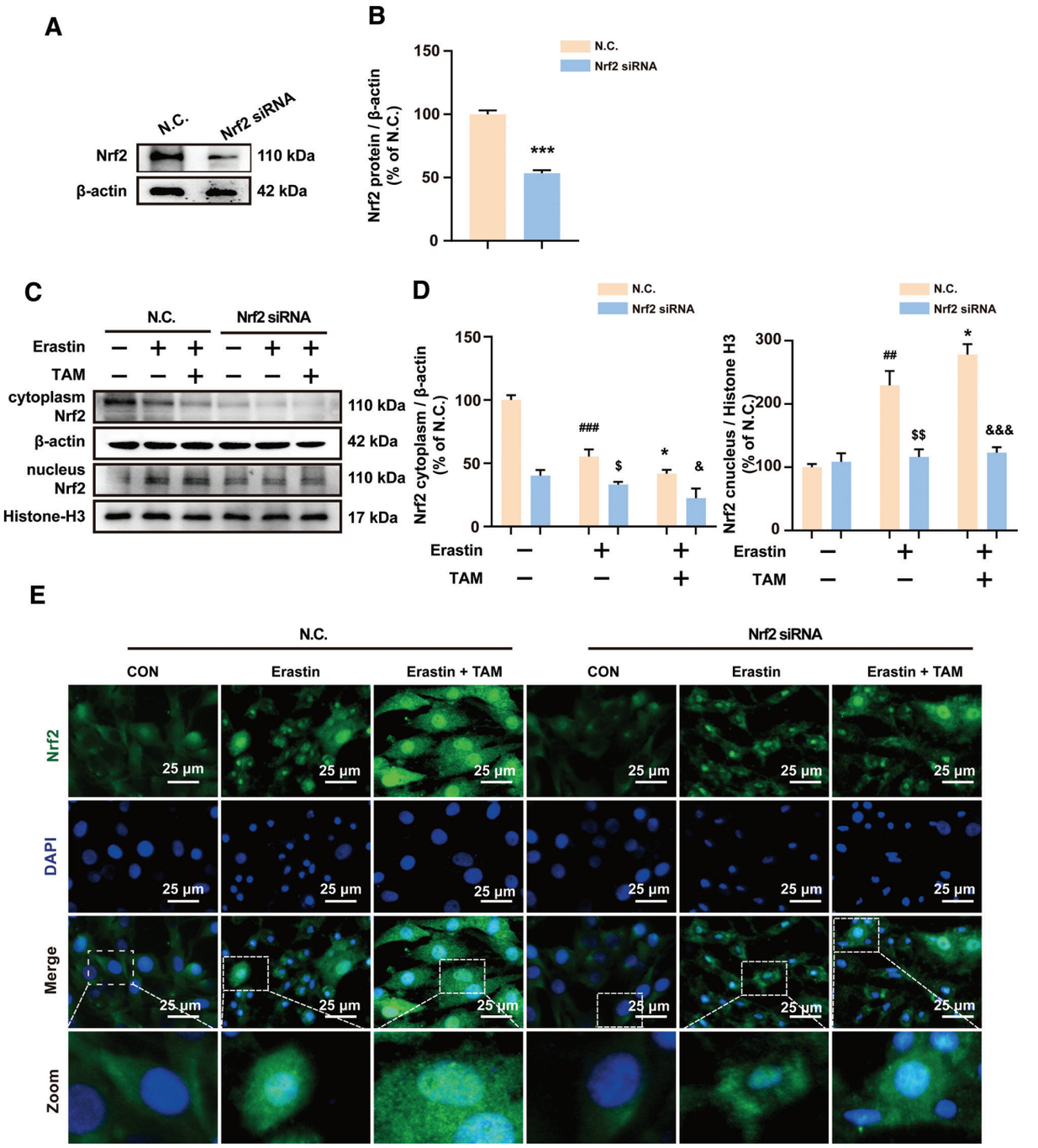

Figure 7. Nrf2 silence weakened the effect of tamarixetin on the enhancement of Nrf2 expression *in vitro*. The efficiency of Nrf2 siRNA was quantified *via* western blotting. Representative image of the Nrf2 immunoblot band is presented, accompanied by statistical analysis (A–B). $N = 3$ in each group. The protein expression and spatial distribution of Nrf2 in SH-SY5Y cells incubated with siRNA were tested *via* western blotting and immunofluorescence staining. Representative images of Nrf2 protein expression and immunofluorescence staining are presented and analyzed (C–E). Data are expressed as mean ± SEM. $^{\#}P < 0.05$, $^{\#\#\#}P < 0.001$ *vs*. control group incubated with negative siRNA; $^{*}P < 0.05$ *vs*. erastin group incubated with negative siRNA; $^{\$}P < 0.05$ *vs*. control group incubated with Nrf2 siRNA; $^{\&}P < 0.05$ *vs*. erastin group incubated with Nrf2 siRNA. SEM: Standard error of mean; siRNA: Small interfering RNA; TAM: Tamarixetin.

or eliminated in Nrf2 siRNA-treated cells, whereas its stimulatory effect on oxidized C11 BODIPY™ levels was absent (Figure 8E–G). These findings provide compelling evidence that the suppressive effect of tamarixetin on lipid peroxidation is mitigated by Nrf2 knockdown. Furthermore, our analysis of the antioxidant capabilities of erastin-treated cells revealed that the upregulation of SOD activity, GSH content, and HO-1 and GPx4 protein expression was significantly reduced after Nrf2 siRNA treatment compared with observations in SH-SY5Y cells treated with negative siRNA (Figure 8H–K). In addition, the stimulatory effects of tamarixetin on these indicators were diminished after Nrf2 siRNA treatment (Figure 8H–K). In summary, Nrf2 knockdown attenuated the inhibitory effects of tamarixetin on ferroptosis *in vitro*.

Discussion

The present study had several interesting findings. First, tamarixetin alleviates neurological dysfunction associated with ischemic stroke, including motor and limb coordination impairment, neurological problems, brain infarction, and substantial neuronal loss. Second, tamarixetin treatment inhibited neuronal ferroptosis by activating the Nrf2 pathway. Notably, our findings indicate that Nrf2 is a direct target protein of tamarixetin that mediates its therapeutic effects. Finally, the inhibitory effect of tamarixetin on neuronal ferroptosis is dependent on the presence of Nrf2.

Ischemic stroke, the most prevalent cerebrovascular disorder in humans, has gained considerable attention owing to its high incidence and mortality[42]. It is characterized by inadequate cerebral blood flow, which triggers a cascade of unpredictable pathological processes and cell death[43]. Upon normalization of the blood supply to the brain, excessive oxygen surpasses the actual demand in ischemic areas, initiating a series of unexpected pathological mechanisms that result in extensive cell death, known as I/R injury[44]. These interconnected processes reinforce each other and ultimately lead to neurological dysfunction. Motor dysfunction and limb coordination impairment are the most common neurological manifestations of ischemic stroke[44–45]. Research has shown the effectiveness of therapeutic strategies aimed at mitigating I/R damage in the ischemic penumbra for ischemic stroke management[45]. Tamarixetin shows promise as an effective treatment for ischemic stroke because of its exceptional pharmacological properties, including diverse bioactivities[23–25], high oral bioavailability[26], and favorable pharmacokinetic characteristics[24,46]. The present study demonstrates that tamarixetin alleviates motor dysfunction, limb coordination impairment, neurological complications, and brain infarction in MCAO/R rats. Our findings also suggest that tamarixetin treatment reduces neuronal loss in ischemic regions, thereby providing a compelling rationale for the observed improvements in motor function and limb coordination. Furthermore, the data showed that tamarixetin ameliorated brain injury in MCAO/R rats, even at low doses, demonstrating superior efficacy to quercetin, the positive control used in this study, across multiple parameters. This might be explained as follows: 1) tamarixetin is a directly methylated metabolite of quercetin and possesses higher bioavailability than that of quercetin; 2) these two compounds exert biological effects through shared mechanisms of action, including antioxidant and anti-inflammatory activities. These findings provide crucial insight into the potential advantages and unique effects of quercetin methylation. Collectively, these data provide evidence for the pharmacological efficacy of tamarixetin in the treatment of ischemic stroke, highlighting its potential as a promising therapeutic agent.

Ferroptosis is a primary mechanism underlying ischemic stroke[47]. Numerous studies have confirmed the effectiveness of ferroptosis inhibitors or iron chelators in reducing neurological damage caused by ischemic stroke[18]. Ferroptosis occurs during the reperfusion phase following ischemia[48]. Reperfusion of brain tissue with excessive oxygen induces lipid ROS production on the cell membrane, ultimately leading to cell membrane disruption and subsequent ferroptosis[42]. After I/R, the endogenous mechanisms responsible for ROS scavenging, such as SOD, GSH, and HO-1, are diminished. ROS overproduction is accompanied by severe lipid peroxidation and high intracellular iron concentration and ASCL4 protein level[49–51]. The presence of free iron accelerates lipid peroxidation and promotes ROS generation, whereas GPX4, SLC7A11, and GSH levels are decreased in animal models of ischemic stroke[9]. Our study revealed that tamarixetin suppressed iron accumulation, which is advantageous for alleviating neurological dysfunction in MCAO/R rats. Moreover, our data showed the ability of tamarixetin to reduce ROS generation and lipid peroxidation in MCAO/R rats and erastin-treated SH-SY5Y cells, which is consistent with previous observations in lipopolysaccharide-treated cells. Tamarixetin upregulated cellular antioxidant capacity, which was evident from the elevation in SOD activity, GSH content, and HO-1 and GPx4 protein expression. These results provide compelling evidence for the inhibitory effect of tamarixetin on neuronal ferroptosis *in vivo* and *in vitro*. Furthermore, our data provide novel evidence supporting the antioxidant activity of tamarixetin. To our knowledge, this is the first study to comprehensively demonstrate that the naturally occurring flavonoid tamarixetin is a potent inhibitor of ferroptosis.

Nrf2 acts as a pivotal cellular regulator within the intricate network governing oxidative stress, neuroinflammation, and ferroptosis, particularly in the aftermath of ischemic stroke[52]. As a modulator of cellular redox responses, Nrf2 is predominantly expressed in brain neurons, forming a cytoplasmic complex with the inhibitory protein Keap1[53]. Nrf2 expression is regulated *via* two primary pathways: the classical pathway, which relies heavily on Keap1 expression[54], and alternative pathway, which depends on Nrf2 phosphorylation[55]. Nrf2 regulates redox homeostasis and iron metabolism. GPx4 reduces cellular sensitivity to ferroptosis, whereas GSH mitigates ROS accumulation and suppresses ferroptosis. Several proteins within the Nrf2 signaling pathway act as direct targets for lipid peroxidation. Keap1 is one of these proteins[56]. Our findings suggest that tamarixetin enhanced Nrf2 expression *via* the classical pathway. This was demonstrated by the downregulation of Keap1 protein expression, promotion of the dissociation between Keap1 and Nrf2, upregulation of Nrf2 expression and its subsequent translocation to

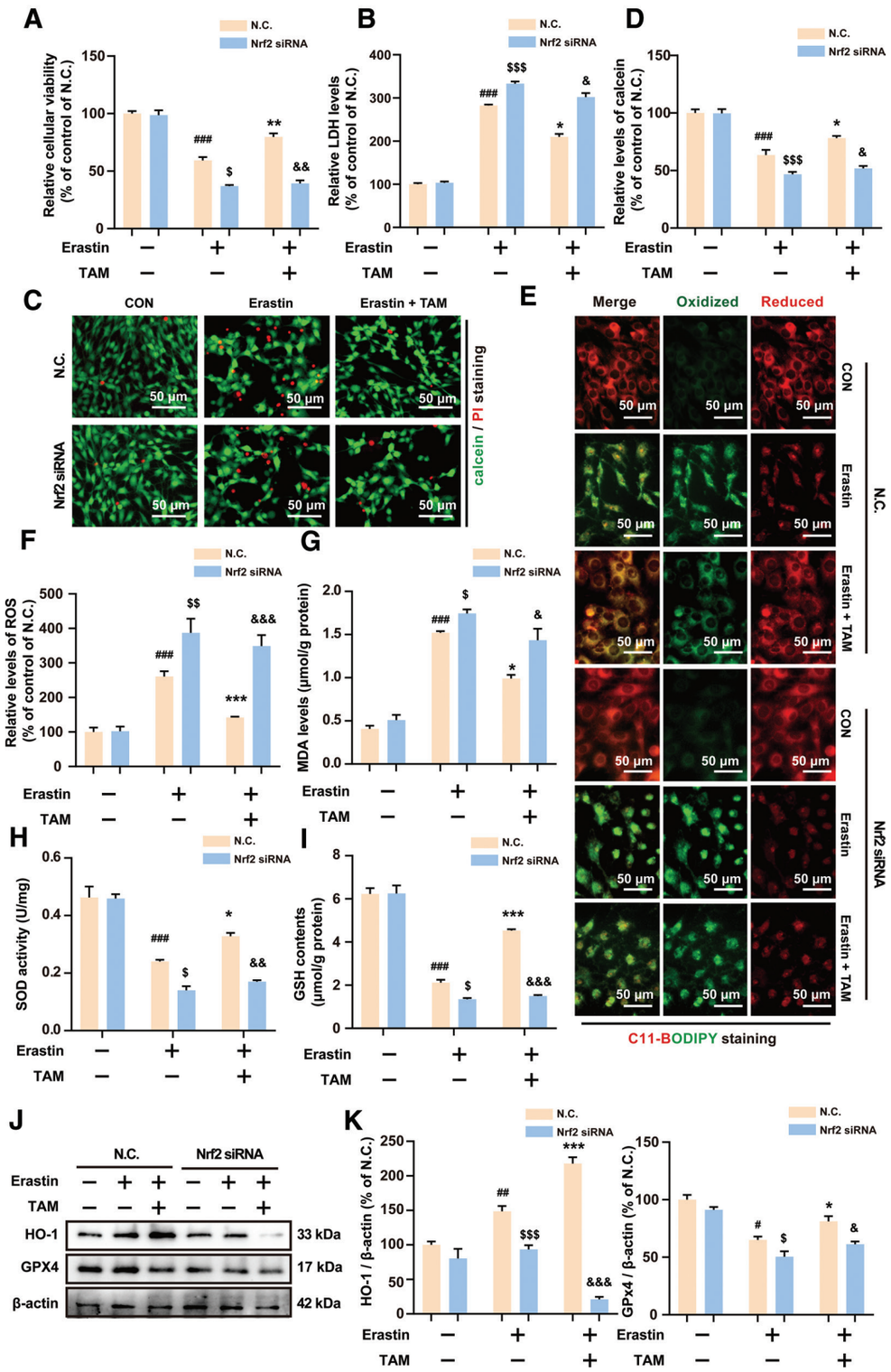

Figure 8. Nrf2 silencing mitigated the protective effect of tamarixetin against neuronal ferroptosis *in vitro*. Calcein AM/PI staining and MTT assay were employed to detect cellular viability. Typical images of calcein AM and PI staining are presented, followed by quantitative analysis (A–B). $N = 3$; scale bar = 100 μm. Detailed data from the MTT assay are presented (C–D), $N = 3$. The ROS levels were evaluated using the C11-BODIPY™ and DCFH-DA probes as well as representative pictures and quantitative analysis (E–F). $N = 3$; scale bar = 100 μm. The MDA content (G), SOD activity (H), and GSH content (I) were quantified using commercial kits. The protein expression of antioxidant enzymes HO-1 and GPx4 was evaluated *via* western blotting. Representative immunoblot bands of HO-1 and GPx4, as well as corresponding statistical analysis, are presented (J–K). $N = 3$ in each group. Data are expressed as mean ± SEM. $^{\#\#}P < 0.01$, $^{\#\#\#}P < 0.001$ *vs*. control group incubated with negative siRNA; $^{*}P < 0.05$, $^{**}P < 0.01$, $^{***}P < 0.001$ *vs*. erastin group incubated with negative siRNA; $^{\$}P < 0.05$, $^{\$\$}P < 0.01$, $^{\$\$\$}P < 0.001$ *vs*. control group incubated with Nrf2 siRNA; $^{\&}P < 0.05$, $^{\&\&}P < 0.01$, $^{\&\&\&}P < 0.001$ *vs*. erastin group incubated with Nrf2 siRNA. DCFH-DA: 2',7'-Dichlorodihydrofluorescein diacetate; GPX4: Glutathione peroxidase 4; HO-1: Heme oxygenase-1; MDA: Malondialdehyde; MTT: 3-(4,5-dimethylthiazol-2-yl)-2,5 diphenyltetrazolium bromide; PI: Propidium iodide; SEM: Standard error of mean; siRNA: Small interfering RNA; SOD: Superoxide dismutase; TAM: Tamarixetin.

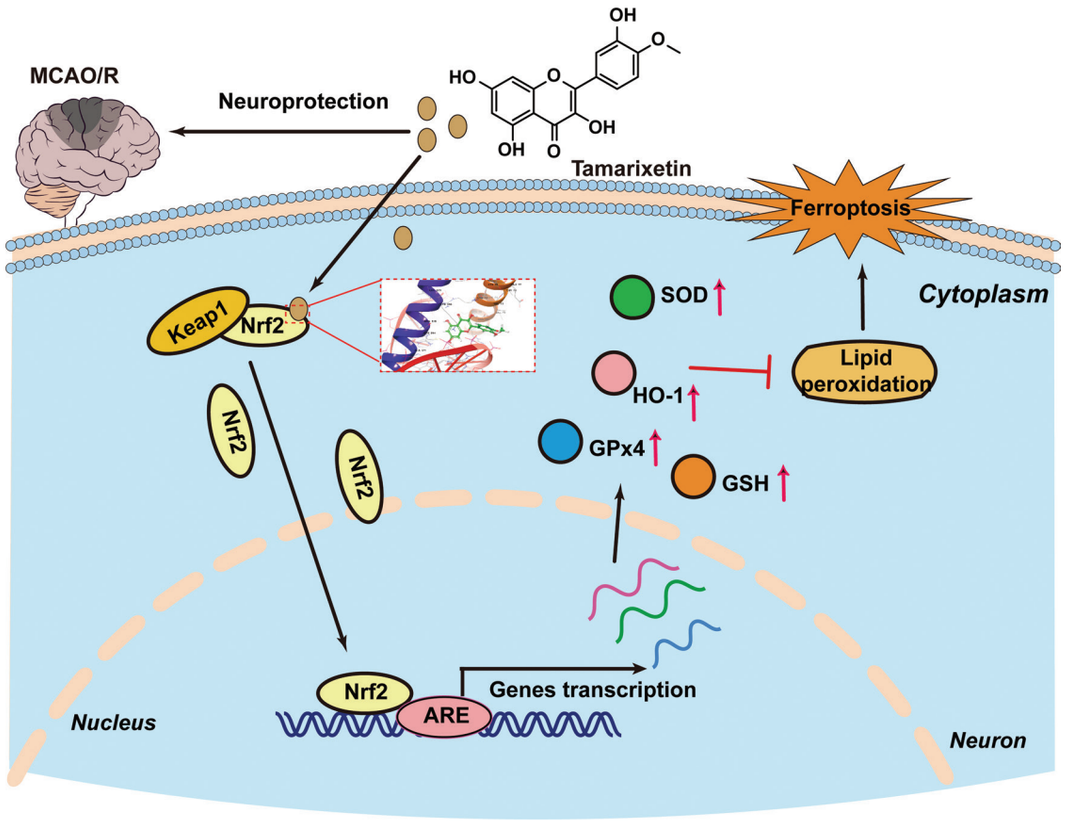

Figure 9. A diagram visually depicting the intricate mechanism of tamarixetin in suppressing neuronal ferroptosis in ischemic stroke. GPX4: Glutathione peroxidase 4; GSH: Glutathione; HO-1: Heme oxygenase-1; MCAO/R: Middle cerebral artery occlusion and reperfusion; SOD: Superoxide dismutase.

the nucleus, and increased levels of antioxidative enzymes. In addition, our data indicated that tamarixetin directly interacts with Nrf2 under cell-free conditions, enhancing its enzymatic and thermal stability. These data reveal a previously unreported mechanism by which tamarixetin directly binds to Nrf2, stabilizes it, and promotes its nuclear translocation, thereby initiating a protective antioxidant response. This distinct mechanism distinguishes tamarixetin from other known ferroptosis inhibitors, such as Fer-1. The discovery of the direct binding of tamarixetin to Nrf2 and its efficacy highlights its significant therapeutic potential. In conclusion, our findings provide initial evidence that tamarixetin directly interacts with Nrf2 and activates its corresponding signaling pathway. Although our study yielded preliminary findings, further comprehensive research is imperative before tamarixetin can be safely used in clinical settings. Further evidence is required to precisely elucidate the intricate interplay between tamarixetin and Nrf2. To achieve this, we will employ innovative methodologies in future experiments, including liquid chromatography–mass spectrometry, point mutation techniques, pull-down assays, and Nrf2 knockout animal models.

All in all, this study demonstrated that tamarixetin alleviates brain damage following ischemic stroke. This remarkable therapeutic enhancement of tamarixetin could be attributed to its ability to suppress neuronal ferroptosis by targeting and augmenting the activation of the Nrf2 pathway (Figure 9). Tamarixetin represents a novel and promising lead compound for the development of targeted therapies against ferroptosis-related conditions, such as ischemic stroke.

Conflict of interest statement

The authors declare no conflict of interest.

Funding

This work is supported by the National Natural Science Foundation of China (82174076), the Construction Project of Liaoning Provincial Key Laboratory, China (2022JH13/10200026), the Natural Science Foundation of Hebei Province (H2024501002), the Fundamental Research Funds for the Central Universities (N2423006), and the 111 Project (B16009).

Author contributions

Yanqiu Yang and Mingxia Fang were the main researchers of this study, taking charge of conducting experiments, collecting data, and writing research manuscripts. Qingqi Meng and Yan Mi aided in the research efforts, while Libin Xu, Hua Guo, and Yueyang Liu provided assistance with statistical analyses of the research data. Mingzhong Li and Nanik Siti Aminah contributed to data management. Zipeng Gong and Yue Hou conceptualized the research objectives, designed methods, and supervised the project. All authors reviewed and edited the final manuscript.

Ethical approval of studies and informed consent

All animal experiments were approved by the Animal and Medical Ethics Committee of Northeastern University (No.: NEU-EC-2025A012S). This article contains no experiments involving human subjects conducted by any of the contributors.

Acknowledgments

None.

Data availability

The data that support the findings of this study are available from the corresponding author upon reasonable request. All data were generated in-house, and no paper mill was used.

Declaration of generative AI in scientific writing

The conception and writing of this article were carried out collaboratively by all authors. Artificial intelligence was utilized exclusively for refining sentence coherence and amending punctuation. All citations in this manuscript were manually searched for and incorporated. After utilizing the aforementioned tools/services, the authors thoroughly reviewed and revised the content and take full responsibility for the entirety of this publication.

References

[1] Dixon SJ, Lemberg KM, Lamprecht MR, et al. Ferroptosis: an iron-dependent form of nonapoptotic cell death. *Cell* 2012;149(5):1060–1072.
[2] Bersuker K, Hendricks JM, Li ZP, et al. The CoQ oxidoreductase FSP1 acts parallel to GPX4 to inhibit ferroptosis. *Nature* 2019;575:688–692.
[3] Zhou B, Liu J, Kang R, et al. Ferroptosis is a type of autophagy-dependent cell death. *Semin Cancer Biol* 2020;66:89–100.
[4] Dixon SJ, Winter GE, Musavi LS, et al. Human haploid cell genetics reveals roles for lipid metabolism genes in nonapoptotic cell death. *ACS Chem Biol* 2015;10:1604–1609.
[5] Latunde-Dada GO. Ferroptosis: role of lipid peroxidation, iron and ferritinophagy. *Biochim Biophys Acta Gen Subj* 2017;1861:1893–1900.
[6] Stockwell BR, Angeli JPF, Bayir H, et al. Ferroptosis: a regulated cell death nexus linking metabolism, redox biology, and disease. *Cell* 2017;171:273–285.
[7] Wen X, Wu J, Wang F, et al. Deconvoluting the role of reactive oxygen species and autophagy in human diseases. *Free Radic Biol Med* 2013;65:402–410.
[8] Kerins MJ, Ooi A. The roles of NRF2 in modulating cellular iron homeostasis. *Antioxid Redox Signal* 2018;29:1756–1773.
[9] Shin D, Kim EH, Lee J, et al. Nrf2 inhibition reverses resistance to GPX4 inhibitor-induced ferroptosis in head and neck cancer. *Free Radic Biol Med* 2018;129:454–462.
[10] Dodson M, Castro-Portuguez R, Zhang DD. NRF2 plays a critical role in mitigating lipid peroxidation and ferroptosis. *Redox Biol* 2019;23:101107.
[11] Ma Q. Role of Nrf2 in oxidative stress and toxicity. *Annu Rev Pharmacol Toxicol* 2013;53:401–426.
[12] Yang X, Park SH, Chang HC, et al. Sirtuin 2 regulates cellular iron homeostasis *via* deacetylation of transcription factor NRF2. *J Clin Invest* 2017;127:1505–1516.
[13] Sun X, Ou Z, Chen R, et al. Activation of the p62-Keap1-Nrf2 pathway protects against ferroptosis in hepatocellular carcinoma cells. *Hepatology* 2016;63:173–184.
[14] Tuo QZ, Lei P, Jackman KA, et al. Tau mediated iron export prevents ferroptotic damage after ischemic stroke. *Mol Psychiatry* 2017;22:1520–1530.
[15] DeGregorio-Rocasolano N, Martí-Sistac O, Gasull T. Deciphering the iron side of stroke: neurodegeneration at the crossroads between iron dyshomeostasis, excitotoxicity, and ferroptosis. *Front Neurosci* 2019;13:85.
[16] Guan X, Li X, Yang X, et al. The neuroprotective effects of carvacrol on ischemia/reperfusion-induced hippocampal neuronal impairment by ferroptosis mitigation. *Life Sci* 2019;235:116795.
[17] Guo J, Tuo QZ, Lei P. Iron, ferroptosis, and ischemic stroke. *J Neurochem* 2023;165:487–520.
[18] Pan YH, Wang XK, Liu XW, et al. Targeting ferroptosis as a promising therapeutic strategy for ischemia-reperfusion injury. *Antioxidants* 2022;11:2196.
[19] Huxley RR, Neil HA. The relation between dietary flavonol intake and coronary heart disease mortality: a meta-analysis of prospective cohort studies. *Eur J Clin Nutr* 2003;57:904–908.
[20] Han DX, Yao YJ, Chen L, et al. Apigenin ameliorates di(2-ethylhexyl) phthalate-induced ferroptosis: the activation of glutathione peroxidase 4 and suppression of iron intake. *Food Chem Toxicol* 2022;164:113089.
[21] Wang C, Lin JH, Lee WS, et al. Baicalein and luteolin inhibit ischemia/reperfusion-induced ferroptosis in rat cardiomyocytes. *Int J Cardiol* 2023;375:74–86.
[22] Shen F, Jiang L, Han F, et al. Increased inflammatory response in old mice is associated with more severe neuronal injury at the acute stage of ischemic stroke. *Aging Dis* 2019;10:12–22.
[23] Hayamizu K, Morimoto S, Nonaka M, et al. Cardiotonic actions of quercetin and its metabolite tamarixetin through a digitalis-like enhancement of Ca^{2+} transients. *Arch Biochem Biophys* 2018;637:40–47.
[24] Moalin M, Van Strijdonck GPF, Bast A, et al. Competition between ascorbate and glutathione for the oxidized form of methylated quercetin metabolites and analogues: tamarixetin, 4'-o-methylquercetin, has the lowest thiol reactivity. *J Agric Food Chem* 2012;60:9292–9297.
[25] Xu J, Cai XH, Teng SS, et al. The pro-apoptotic activity of tamarixetin on liver cancer cells *via* regulation mitochondrial apoptotic pathway. *Appl Biochem Biotechnol* 2019;189:647–660.
[26] Shen JY, Jia Q, Huang XH, et al. Study on pharmacokinetic and bioavailability of tamarixetin after intravenous and oral administration to rats. *Evid Based Complement Alternat Med* 2019;2019:6932053.
[27] Sun YJ, Li J, Georgi R, et al. Effects of acupuncture on angiogenesis-associated factor expression in ischemic brain tissue following cerebral infarction in rats. *Acupunct Herb Med* 2023;3(1):46–54.
[28] Pan C, Liu N, Zhang P, et al. EGb761 ameliorates neuronal apoptosis and promotes angiogenesis in experimental intracerebral hemorrhage *via* rSK1/GSK3beta pathway. *Mol Neurobiol* 2018;55:1556–1567.
[29] Kinoshita K, Ohtomo R, Takase H, et al. Different responses after intracerebral hemorrhage between young and early middle-aged mice. *Neurosci Lett* 2020;735:135249.
[30] Takamatsu Y, Tamakoshi K, Waseda Y, et al. Running exercise enhances motor functional recovery with inhibition of dendritic regression in the motor cortex after collagenase-induced intracerebral hemorrhage in rats. *Behav Brain Res* 2016;300:56–64.
[31] Sui RB, Zang L, Bai YJ. Administration of troxerutin and cerebroprotein hydrolysate injection alleviates cerebral ischemia/reperfusion injury by down-regulating caspase molecules. *Neuropsychiatr Dis Treat* 2019;15:2345–2352.
[32] Nie Y, Huang MY, Yang TY, et al. Ferulic acid reduces inflammatory response induced by radiation through Sirt1-NLRP3 pathway. *Acupunct Herb Med* 2024;4(3):367–374.
[33] Wang CY, Zhang Q, Xun Z, et al. Increases of iASPP-Keap1 interaction mediated by syringin enhance synaptic plasticity and rescue cognitive impairments *via* stabilizing Nrf2 in Alzheimer's models. *Redox Biol* 2020;36:101672.
[34] Hu C, Zhang X, Wei WY, et al. Matrine attenuates oxidative stress and cardiomyocyte apoptosis in doxorubicin-induced cardiotoxicity *via* maintaining AMPK α/UCP2 pathway. *Acta Pharm Sin B* 2019;9:690–701.
[35] Yang Y, Hao T, Yao X, et al. Crebanine ameliorates ischemia-reperfusion brain damage by inhibiting oxidative stress and neuroinflammation mediated by NADPH oxidase 2 in microglia. *Phytomedicine* 2023;120:155044.
[36] Yang Y, Chen R, Che Y, et al. Isoamericanin A improves lipopolysaccharide-induced memory impairment in mice through suppression of the nicotinamide adenine dinucleotide phosphateoxidase-dependent nuclear factor kappa B signaling pathway. *Phytother Res* 2023;37:3982–4001.
[37] Liu Z, Nan P, Gong Y, et al. Endoplasmic reticulum stress-triggered ferroptosis *via* the XBP1-Hrd1-Nrf2 pathway induces

EMT progression in diabetic nephropathy. *Biomed Pharmacother* 2023;164:114897.
[38] Zhang XW, Feng N, Liu YC, et al. Neuroinflammation inhibition by small-molecule targeting USP7 noncatalytic domain for neurodegenerative disease therapy. *Sci Adv* 2022;8:eabo0789.
[39] Yang H, Liu Y, Zhao MM, et al. Therapeutic potential of targeting membrane spanning proteoglycan SDC4 in hepatocellular carcinoma. *Cell Death Dis* 2021;12:492.
[40] Hao T, Yang Y, Li N, et al. Inflammatory mechanism of cerebral ischemia-reperfusion injury with treatment of stepharine in rats. *Phytomedicine* 2020;79:153353.
[41] Zeng K, Wang J, Wang L, et al. Small molecule induces mitochondrial fusion for neuroprotection *via* targeting CK2 without affecting its conventional kinase activity. *Signal Transduct Target Ther* 2021;6(1):71.
[42] Deng XM, Chu WM, Zhang HR, et al. Nrf2 and ferroptosis: a new research direction for ischemic stroke. *Cell Mol Neurobiol* 2023;43:3885–3896.
[43] Walter K. What is acute ischemic stroke? *JAMA* 2022;327:885.
[44] Gauberti M, Lapergue B, Martinez de Lizarrondo S, et al. Ischemia-reperfusion injury after endovascular thrombectomy for ischemic stroke. *Stroke* 2018;49:3071–3074.
[45] Ángel C, Ulrich D, Xabier U, et al. Neuroprotection in acute stroke: targeting excitotoxicity, oxidative and nitrosative stress, and inflammation. *Lancet Neurol* 2016;15:869–881.
[46] Kumari A, Yadav SK, Pakade YB, et al. Development of biodegradable nanoparticles for delivery of quercetin. *Colloids Surf B Biointerfaces* 2010;80:184–192.
[47] Xu Y, Li K, Zhao Y, et al. Role of ferroptosis in stroke. *Cell Mol Neurobiol* 2023;43:205–222.
[48] Tang L, Luo X, Tu H, et al. Ferroptosis occurs in phase of reperfusion but not ischemia in rat heart following ischemia or ischemia/reperfusion. *Naunyn Schmiedebergs Arch Pharmacol* 2021;394:401–410.
[49] Zhao Y, Xin Z, Li N, et al. Nano-liposomes of lycopene reduces ischemic brain damage in rodents by regulating iron metabolism. *Free Radic Biol Med* 2018;124:1–11.
[50] Scindia Y, Leeds J, Swaminathan S. Iron homeostasis in healthy kidney and its role in acute kidney injury. *Semin Nephrol* 2019;39:76–84.
[51] Dawi J, Affa S, Gonzalez E, et al. Ferroptosis in cardiovascular disease and cardiomyopathies: therapeutic implications of glutathione and iron chelating agents. *Biomedicines* 2024;12(3):558.
[52] Wang L, Zhang X, Xiong X, et al. Nrf2 regulates oxidative stress and its role in cerebral ischemic stroke. *Antioxidants (Basel)* 2022;11:2377.
[53] Ungvari Z, Bagi Z, Feher A, et al. Resveratrol confers endothelial protection *via* activation of the antioxidant transcription factor Nrf2. *Am J Physiol Heart Circ Physiol* 2010;299:H18–H24.
[54] Zhang R, Xu M, Wang Y, et al. Nrf2, a promising therapeutic target for defensing against oxidative stress in stroke. *Mol Neurobiol* 2017;54(8):6006–6017.
[55] Zhu Z, Wang Y, Deng Z, et al. The Hemerocallis citrina extracts ameliorate radiation-induced ferroptosis in LO2 cells through the Nrf2-xCT/GPX4 pathway. *Acupunct Herb Med* 2024;4(4):513–524.
[56] Dinkova-Kostova AT, Kostov RV, Canning P. Keap1, the cysteine-based mammalian intracellular sensor for electrophiles and oxidants. *Arch Biochem Biophys* 2017;617:84–93.